A biomimetic peptide has no effect on the isotopic fractionation during *in vitro* silica precipitation

Lucie Cassarino[1,*], Paul Curnow[2,+], and Katharine R. Hendry[1,+]

[1]University of Bristol, School of Earth Sciences, Wills Memorial Building, Queen's Road, Brsitol, BS8 1RJ, UK
[2]University of Bristol, School of Biochemistry, Medical Sciences Building, University Walk, Bristol BS8 1TD, UK
[*]corresponding.l.cassarino@bristol.ac.uk
[+]these authors contributed equally to this work

ABSTRACT

The stable isotopic composition of diatom silica is used as a proxy for nutrient utilisation in natural waters. This approach provides essential insight into the current and historic links between biological production, carbon cycling and climate. However, estimates of isotopic fractionation during diatom silica production from both laboratory and field studies are variable, and the biochemical pathways responsible remain unknown. Here, we investigate silicon isotopic fractionation through a series of chemical precipitation experiments that are analogous to the first stages of intracellular silica formation within the diatom silicon deposition vesicle. The novelty of our experiment is the inclusion of the R5 peptide, which is closely related to a natural biomolecule known to play a role in diatom silicification. Our results suggest that the presence of R5 induces a systematic but non-significant difference in fractionation behaviour. It thus appears that silicon isotopic fractionation *in vitro* is largely driven by an early kinetic fractionation during rapid precipitation that correlates with the initial amount of dissolved silica in the system. Our findings raise the question of how environmental changes might impact silicon isotopic fractionation in diatoms, and whether frustule archives record information in addition to silica consumption in surface water.

Introduction

Silicon (Si) is an important nutrient in the biology of organisms such as diatoms, sponges, radiolarians and silicoflagellates. These organisms are capable of a process known as biosilicification, in which solid silica is precipitated in a controlled manner from dissolved silicon (dSi) acquired from the environment. Marine diatoms are generally heavily silicified, and are of particular interest since they are responsible for about 40% of primary production and a significant proportion of carbon export to the seafloor[1]. Many diatom species require Si for cell growth, meaning that there is a direct link between the global silica cycle, carbon uptake and climate change[2–4].

Diatoms are encased in an outer cell wall, or frustule, made of hydrated amorphous silica ($SiO_2{\cdot}nH_2O$). This is often referred to as opal or biogenic silica (BSi)[5]. The process of diatom silicification is still not well-understood, but it appears to occur inside the cell through a series of tightly-controlled, coordinated and interdependent steps. Figure 1 briefly summarizes the pathway of silicification in the diatom. The porous silicified outer cell wall (frustule) is formed of two overlapping halves (thecae). Soluble silica in the environment as monomeric silicic acid, $Si(OH)_4$, moves through the porous frustule and across the underlying plasma membrane via passive or active transport. The cellular Si pool, which can approach high millimolar concentrations, is likely balanced by efflux processes[6]. This accumulated soluble silica is then transferred to the intracellular silicon deposition vesicle (SDV) which is the site of frustule formation. The SDV is likely to be a golgi-derived vesicle with an acidic lumen[7]. Biomineralisation occurs within the SDV through polymerisation[8]. The SDV contains genetically-encoded[9], species-specific biomolecules that are thought to support and direct silica biosynthesis, and which are found intimately associated with the mature frustule. These biomolecules are represented as geometric shapes in Figure 1 and include long-chain polyamines[10], as well as the different peptides known as silaffins, silacidins and frustulins[11–13]. Other factors, such as the SDV membrane and the cytoskeleton, are also thought to be critical in forming the structure of the frustule[8] but are not shown or discussed further here. The final stage of silicification involves the export of the nascent frustule to the cell exterior and subsequent maturation. While these general principles of biomineralisation are known to a certain degree, many of the specific processes underlying them remain poorly understood.

Previous studies have attempted to understand the role of silica-associated biomolecules by studying their ability to influence the formation of silica *in vitro*. An attractive model system in this regard is the peptide known as 'R5', which has the

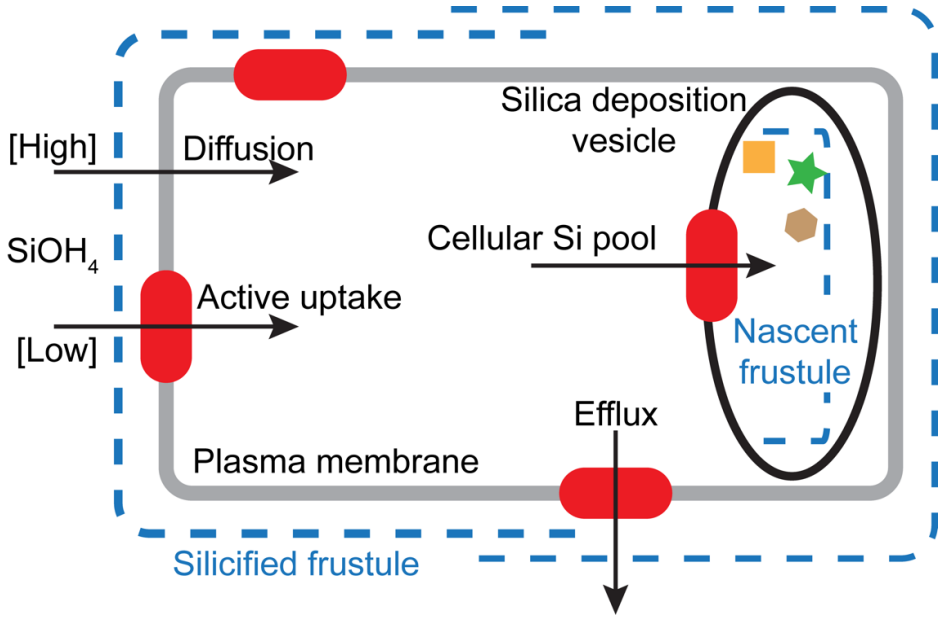

Figure 1. Schematic cartoon of silica formation in the diatom. Soluble silicic acid enters the diatom cell through active or passive transport and is moved to the silica deposition vesicle (SDV) via intracellular Si pools. The SDV is the site of frustule synthesis and the nascent frustule forms in the presence of various biomolecules, shown here as geometric shapes. See text for details.

sequence NH_2-SSKKSGSYSGSKGSKRRIL-CO_2H and was derived from the sequence of a silaffin peptide from *Cylindrotheca fusiformis*[14]. The native silaffin on which R5 is based is rather complex, featuring extensive and unusual posttranslational modifications, and must be extracted from diatom silica[14,15]. In contrast, R5 can be obtained easily by facile peptide synthesis. The major drawback of using R5 is that while the native silaffins are highly active at low pH, consistent with the likely environment of the SDV lumen, the synthetic R5 peptide is only active at pH >7[12,16]. Nonetheless R5 has found favour as a tractable surrogate for understanding how short, charged peptides might influence silicification[17–21].

One interesting aspect of biosilica formation in the diatoms is the bias towards lighter isotopes of silicon within the mineral[22–26]. This preferential incorporation of the light isotope (^{28}Si) leaves the heavy isotopes (^{29}Si and ^{30}Si) in the surrounding seawater. This phenomenon is sufficiently robust that it can be used as a proxy for the biological consumption of dSi by key producers such as diatoms[24,26,27]. Measuring the Si isotopic composition (δ^{30}Si) of laboratory diatom cultures, samples from the modern ocean and sedimentary archives has thus provided a deeper understanding of the role of diatoms in the past and present Si cycle[28–31]. However, the biological mechanisms and pathways driving the fractionation of Si isotopes during biomineralisation are as yet unknown.

The true isotopic fractionation factor of diatom silica α is defined as:

$$\alpha_{A-B} = \frac{R_A}{R_B} \tag{1}$$

where R = ^{30}Si / ^{28}Si of component A (diatom) and B (dSi in seawater). This can also be expressed as the apparent fractionation factor, which is the difference between the Si isotopic composition of the diatoms and the seawater ($\Delta^{30}Si_{p\text{-}s}$ = $\delta^{30}Si_{diatom}$ - $\delta^{30}Si_{dSi}$). Two models are commonly applied to determine the fractionation factor (ε) value from either laboratory or field data: the Rayleigh model (single input of silicic acid to a stratified system) and the open system model (continuous flux of silicic acid to a mixed system[22]). To date we have successfully used both Si isotopic fractionation models to study the role of organisms such as diatoms, sponges and choanoflagellates[26,32] in the global Si cycle.

Several lines of evidence now point to both genetic and environmental control of isotope fractionation. Although early work reported consistent fractionation factors of ε = -1.1‰[22], more recent studies have reported a range of fractionation factors across different diatom species (-2.09 ‰ to -0.54‰)[33]. The composition of other biosilicas, for example from sponges, is also markedly different from that of the diatoms, despite the mineral being chemically equivalent[32]. The same species of diatom can also display different degrees of fractionation depending upon the ambient conditions[33,34]. The interplay between environmental conditions and biochemical pathways that control fractionation is thus of keen interest for the basic understanding of diatom biology and for the robust interpretation of sedimentary geochemical archives of past ocean change.

A reasonable starting point is the assumption that fractionation might be occurring at the point of silica precipitation in the SDV, since this involves intimate engagement of the forming mineral with a complex assortment of biomacromolecules. The SDV has evaded detailed characterisation for decades, so we chose instead to study Si isotopic fractionation using the R5 model for silica precipitation *in vitro*. We investigated here whether the presence of R5 during Si precipitation was able to influence the Si isotopic composition of the resulting silica when compared with an abiological control. We find that the presence of R5 does induce a systematic but non-significant difference in fractionation behaviour. Our results suggest instead that the isotopic composition of silica is largely driven by an early kinetic fractionation during rapid precipitation. These findings imply that the SDV could be a site of Si isotopic fractionation within the diatom cell, and that this fractionation may not be substantially affected by co-precipitation with organic macromolecules.

Results

Equilibrium versus kinetic fractionation

Silica precipitation was induced by diluting sodium silicate from commercial stock solution into a well-defined saline buffer known as ND96 (see Methods). We chose this particular buffer solution because it maintained a pH range in which R5 was active, included several biological salts, and, importantly, our initial tests confirmed that the buffer matrix did not interfere with the mass spectrometry analysis. The ND96 solutions were confirmed to have $\delta^{30}Si_{dSi}$ very close to 0 ‰. As expected, silica precipitation in this buffer was instantaneous at Si concentrations above 2mM, which is the known saturation point of silica. The precipitated silica was isolated at various timepoints by low-speed centrifugation, generating two fractions: a silica pellet, and a supernatant containing buffer salts and the remaining soluble Si. Measurement of soluble Si by molybdate assay was performed after sub-sampling event and at the end of the experiments both fractions were sub-sampled for Si isotopic analysis.

In a first set of experiments, the precipitation reaction was incubated for 8 days before the pellet and supernatant fractions were obtained and analysed. We assume that this is sufficient time for the reaction to have reached chemical equilibrium (i.e. have attained an overall constant dSi concentration) and equilibrium isotopic fractionation (attained a constant rate of isotopic two way transfer between precipitate and solution) and so refer to these data as being at 'equilibrium'. In a second set of experiments we separated the precipitate 1h after mixing. We assume that these samples have not yet attained complete thermodynamic equilibrium and so refer to this as a 'kinetic' experiment. Figure 2 shows the Si isotopic fractionation between the precipitate and the solution of these equilibrium and kinetic experiments. This is presented as a function of the relative Si loss from the initial starting concentration (3.7 – 743mM) due to precipitation (relative Si loss = (initial Si concentration - Si after precipitation) / initial Si concentration).

In the equilibrium experiments, the silica precipitate generally had a negative $\delta^{30}Si$ ($\delta^{30}Si_p$) and the soluble Si had a positive $\delta^{30}Si$ ($\delta^{30}Si_s$), indicating the preferential incorporation of lighter isotopes into the precipitate. This can be expressed as $\Delta^{30}Si_{p\text{-}s}$ which is the difference between $\delta^{30}Si_p$ and $\delta^{30}Si_s$, and generally gives a negative number during silica precipitation[35–37]. The starting concentrations above 148mM resulted in a $\Delta^{30}Si_{p\text{-}s}$ equal to 0 ‰ or positive. Since the dilutions of alkaline sodium silicate required to reach these concentrations resulted in a basic pH > 10, and both samples remained supersaturated in Si with DSi > 99mM, these were excluded and 148mM was set as our upper concentration limit. As expected, in all other equilibrium experiments the concentration of dSi remaining in the supernatant was just above the saturating concentration of 2mM, and pH was consistently maintained in the range 7.7 – 8.8.

In contrast, the kinetic experiments showed a range of supernatant dSi concentrations (2 – 10.3mM), indicating that in most cases we had successfully stopped precipitation before reaching a chemical equilibrium. The pH of the supernatant was between 7.4 and 7.9. The Si isotopic fractionation in these samples followed the same trend as for the equilibrium samples, with preferential precipitation of the light Si isotopes. In comparison with the equilibrium experiment, here the $\Delta^{30}Si_{p\text{-}s}$ shows a continuous trend towards more negative $\Delta^{30}Si_{p\text{-}s}$ values with the relative amount of Si lost from the starting solution. Previous studies have shown that pH can impact the stability and structure of silica precipitates[38], and that at high pH (pH $\sim$ 9) the Si isotope exchange rate between precipitate and solution is higher, and so can affect the fractionation of Si isotopes by over 1 ‰[39]. Figure 3 shows the relationship between pH and $\Delta^{30}Si_{p\text{-}s}$ for both equilibrium and kinetic experiments. The equilibrium experiment shows a negative correlation between pH and $\Delta^{30}Si_{p\text{-}s}$ for pH < 7.7 and is followed by a positive relationship for pH > 7.7. In contrast the kinetic experiments have a narrower range of pH and do not show any obvious link between pH and $\Delta^{30}Si_{p\text{-}s}$. The lack of correlation between pH and $\Delta^{30}Si_{p\text{-}s}$ (Figure 3) indicates that the range of pH across our experiments does not contribute significantly to the $\Delta^{30}Si_{p\text{-}s}$ results.

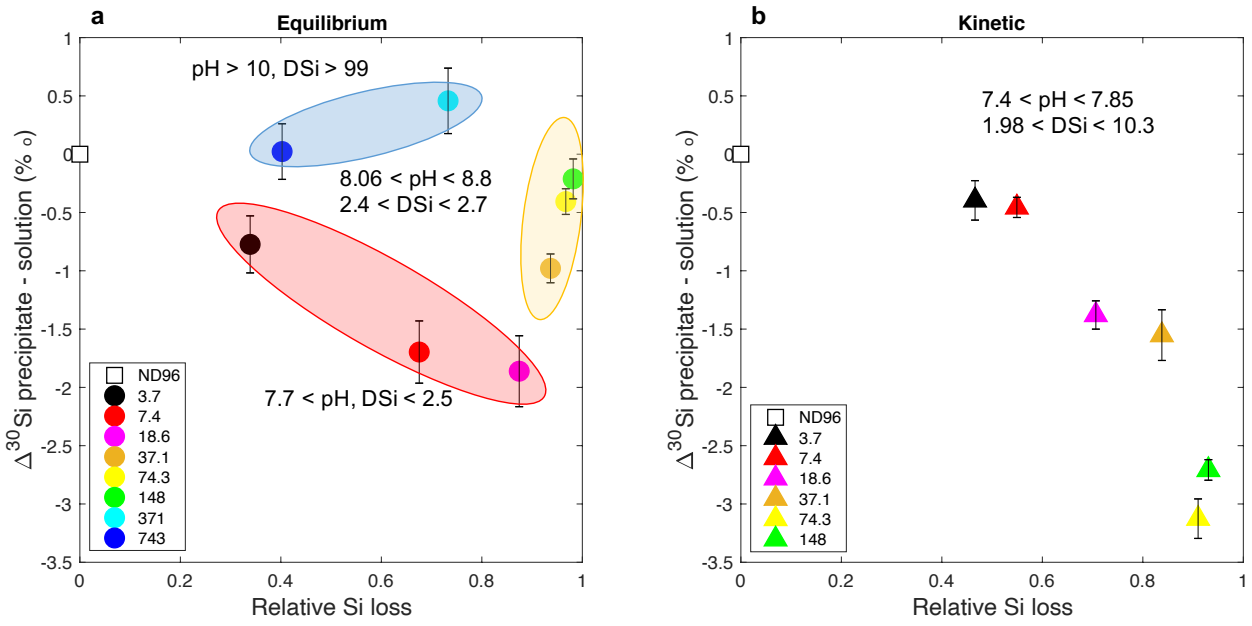

Figure 2. Si isotopic fractionation ($\Delta^{30}Si_{p\text{-}s}$) as a function of the relative silicon loss from solution due to precipitation for a range of dissolved Si concentrations (mM). (a) Experiments after 8 days incubation. (b) Experiments after 1h incubation. Each data point represents a different initial starting concentration of Si, coloured according to the key shown in each panel. Shaded areas in each panel group samples by comparable final conditions as shown. Error bars shows the 2 s.d. of the repeated measurements. Data are also presented in Table 1 in the supplementary information (SI).

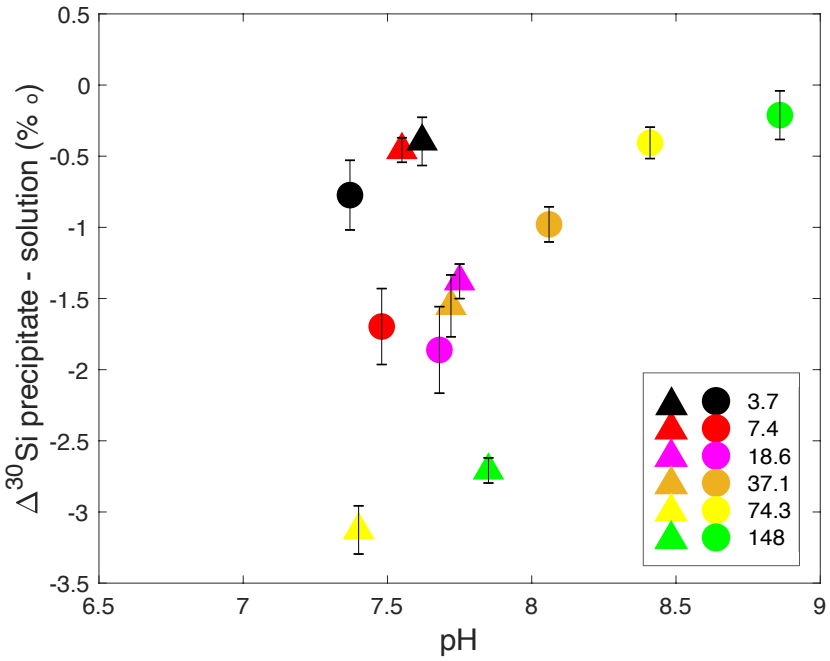

Figure 3. Si isotopic fractionation ($\Delta^{30}Si_{p\text{-}s}$) as a function of pH during the initial kinetic (triangles) reaction and at equilibrium (circles) for the range of dissolved Si concentrations 3.7 - 148mM. Data are also presented in Table 1 in SI.

Precipitation rate and the influence of biomolecules

We next investigated the impact of a mineralising macromolecule, R5, on Si isotopic fractionation. Figure 4 shows the variation in Si precipitation and $\Delta^{30}Si_{p\text{-}s}$ for the abiotic (no R5) and biomimetic (R5) reactions at four concentration regimes over time.

Data for dSi under abiotic conditions are from the colorimetric molybdate assay for soluble silica. dSi concentrations could not be determined using a colorimetric assay for the biomimetic experiment because the R5 peptide reacted with the molybdate reagent, and so were extrapolated from the Multi Collector Induced Coupled Plasma Mass-Spectrometer (MC-ICP-MS) voltages. Figure 4 also shows the best fit and the 95% confidence bounds considering data point error of the abiotic and biomimetic (R5) $\Delta^{30}Si_{p\text{-}s}$ data series, with the best fits following the exponential function $f(x) = a \cdot \exp^{(-bx)}$, which is in accordance with the temporal isotopic fractionation evolution of other light isotope systems during precipitation[40]. Table 1 presents the equations and error for the best fit from Figure 4.

Table 1. Results of the curve fitting of the Si isotopic fractionation during precipitation ($\Delta^{30}Si_{p\text{-}s}$) over time for the abiotic and the biomimetic (R5) experiment.

Initial dSi	Abiotic	Biomimetic (R5)
18.6mM	$\Delta^{30}Si_{p\text{-}s} = -1.67 \cdot \exp^{(-0.21\ day)}$ $r^2 = 0.96$, RMSE = 0.05	$\Delta^{30}Si_{p\text{-}s} = -2.31 \cdot \exp^{(-0.07\ day)}$ $r^2 = 0.97$, RMSE = 0.03
37.1mM	$\Delta^{30}Si_{p\text{-}s} = -2.06 \cdot \exp^{(-0.41\ day)}$ $r^2 = 0.98$, RMSE = 0.03	$\Delta^{30}Si_{p\text{-}s} = -1.81 \cdot \exp^{(-0.19\ day)}$ $r^2 = 0.97$, RMSE = 0.02
74.3mM	$\Delta^{30}Si_{p\text{-}s} = -2.40 \cdot \exp^{(-0.69\ day)}$ $r^2 = 0.99$, RMSE = 0.03	$\Delta^{30}Si_{p\text{-}s} = -2.29 \cdot \exp^{(-0.63\ day)}$ $r^2 = 0.90$, RMSE = 0.07
148mM	$\Delta^{30}Si_{p\text{-}s} = -3.31 \cdot \exp^{(-0.86\ day)}$ $r^2 = 0.99$, RMSE = 0.05	$\Delta^{30}Si_{p\text{-}s} = -3.11 \cdot \exp^{(-1.43\ day)}$ $r^2 = 0.98$, RMSE = 0.09

These data show that the addition of R5 generally resulted in a more consistent dSi loss for the range of concentrations tested, over the timescales of days (Figure 4). However, this might simply be a function of the different ways that dSi was determined in these samples. Initially (day 0 and 1), $\Delta^{30}Si_{p\text{-}s}$ was marginally less pronounced (less negative) in the samples containing R5. After the first day, fractionation was consistently slightly higher (more negative) in the samples containing R5 except for the 18mM. This suggests that the presence of R5 could subtly increase isotopic fractionation during silica formation over the shortest timescales tested. The exception to this was at the highest dSi concentration, where fractionation in the presence of R5 was less than in the abiological sample. Despite these systematic observations, the experiments with and without R5 are not significantly different over the all length of the precipitation (within 95% confidence bounds). Overall, then, our experiments suggest that the presence or absence of R5 makes little difference to the initial fractionation or subsequent exchange behaviour of silica *in vitro*.

Figure 5 focuses on the difference between the early (kinetic, day = 0) and late (equilibrium, day = 10) phase of the precipitation presented in Figure 4. During the kinetic phase $\Delta^{30}Si_{p\text{-}s}$ and the Si concentration (from silica addition) are negatively correlated for both the abiotic and the biomimetic (R5) experiments. In contrast, at steady state, $\Delta^{30}Si_{p\text{-}s}$ and Si are positively correlated. During both phases, there is a consistent but non-significant difference of 0.14 ‰ between abiotic $\Delta^{30}Si_{p\text{-}s}$ and R5 $\Delta^{30}Si_{p\text{-}s}$.

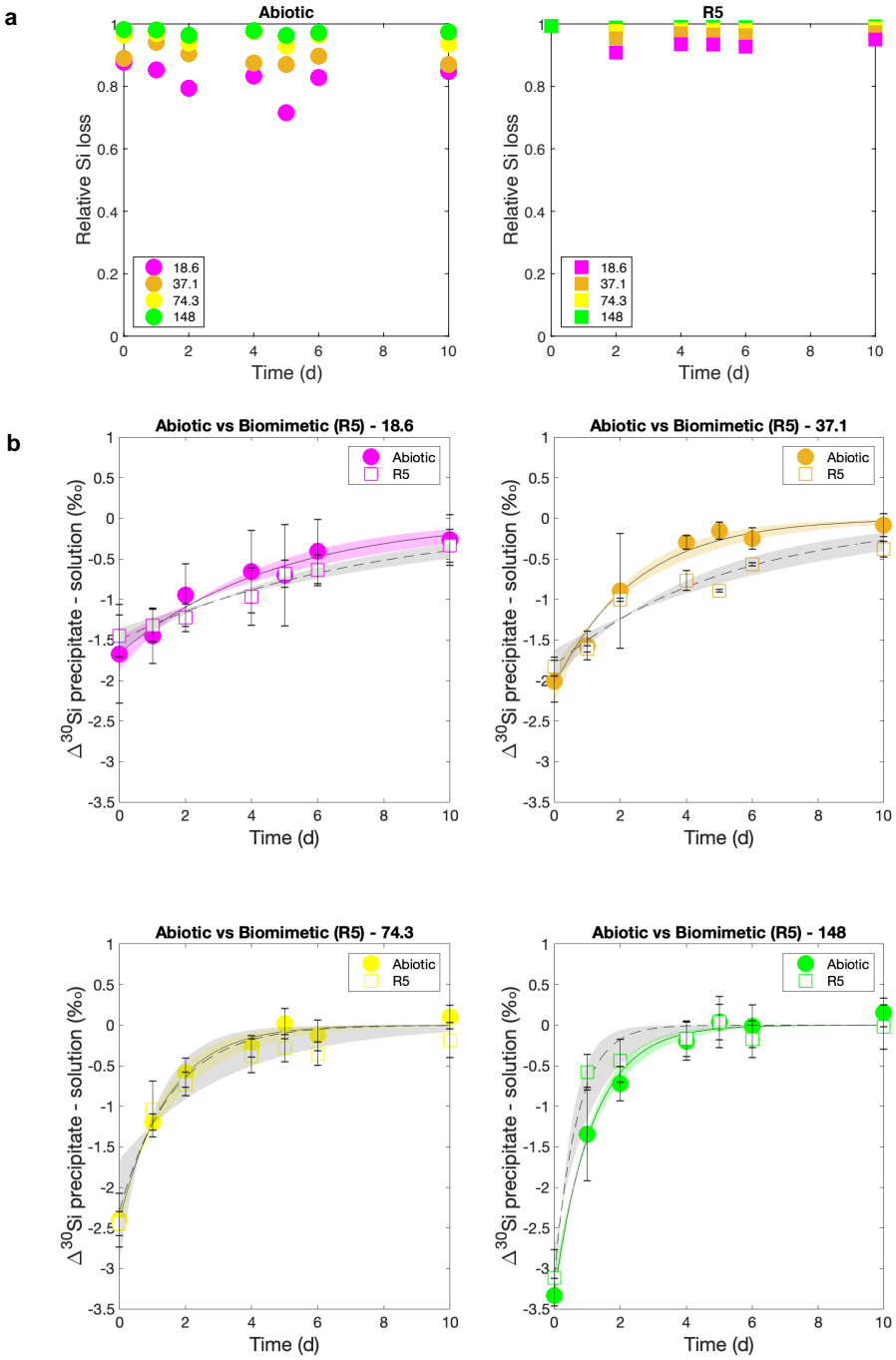

Figure 4. a) Relative Si loss and b) Si isotopic fractionation ($\Delta^{30}Si_{p\text{-}s}$) as a function of time comparing the abiotic (circles) and biomimetic (squares) experiment for initial dSi concentration of 18.6 mM (pink), 37.1 mM (orange), 74.3 mM (yellow) and 148 mM (green). Solid and dashed lines show the best fit (f(x)=a exp(-bx)) with the 95% confidence bounds for the abiotic (coloured) and biomimetic (grey) experiments, respectively. The results of curve fitting are presented in Table 1 and data are also presented in Table 2 and Table 3 in SI.

Discussion

The new experimental data presented here further support observations that simple chemical systems can reproduce the Si isotopic fractionation factors observed in diatom silica[24,26,33,41,42]. Our results confirm that lighter isotopes of Si are

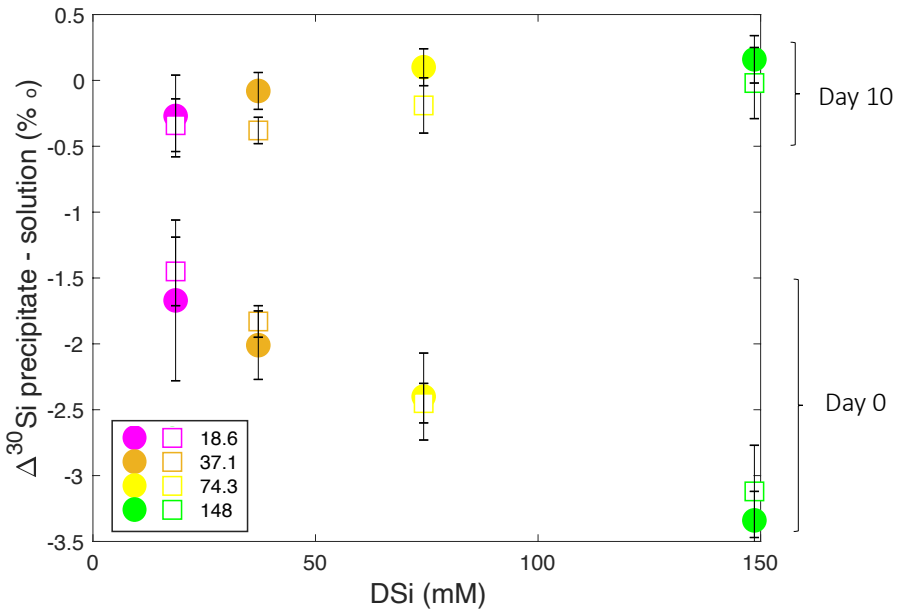

Figure 5. Apparent Si isotopic fractionation ($\Delta^{30}Si_{p\text{-}s}$) of the initial kinetic reaction (day 0) and at steady state (day 10) for the abiotic (circles) and biomimetic (squares) precipitation for the four different Si concentrations, 18.6mM (pink), 37.1mM (orange), 74.3mM (yellow) and 148mM (green). Data are also presented in Table 2 and Table 3 in SI.

preferentially incorporated into silica during the process of precipitation, and we reproduce the change from initial isotopic kinetic fractionation toward equilibrium exchange that has previously been observed for Si and in other isotope systems[35,36,40]. Our results are also in accordance with Oelze et al., 2014 since the extent of the initial kinetic fractionation is inversely correlated to the relative Si loss (Figure 2), i.e. the greater the proportion of the initial dSi that precipitates, the greater the observed fractionation will be. This means that fractionation is more pronounced for samples with higher initial starting concentrations of Si (Figure 4, Table 1).

The presence of various macromolecules, such as charged peptides like R5, could potentially influence Si isotope fractionation on biologically-relevant timescales. This is reinforced by the observation that the addition of R5 can increase the rate and yield of silica precipitation[16]. However, in the model system employed here we found no signficant change in fractionation behaviour upon the addition of R5. This observation suggests that Si concentration alone could be the dominant factor in Si isotopic fractionation within the diatom cell. The length of time required for the initial fractionation to revert to $\Delta^{30}Si_{p\text{-}s} \approx 0$ is also concentration-dependent, being faster in samples with the highest initial concentrations of Si (Figure 4). Nonetheless exchange is relatively slow, and presumably frustule biosilica is moved from the SDV to the cell exterior before such exchange behaviour can happen *in vivo*.

Intriguingly, the range of the kinetic $\Delta^{30}Si_{p\text{-}s}$ values at day 0 and day 1 (-0.58 ‰ – -3.34 ‰, Figure 4b) are in line with values of $\Delta^{30}Si_{p\text{-}s}$ from field or culture studies of diatom silica[22,23,33,41]. These results imply that at least some of the variation found in these cellular studies comes from changes to Si concentration within the SDV. It is assumed that environmental conditions will influence the uptake and distribution of Si within the diatom cell[6], and so this could lead to variability in Si concentration at the site of precipitation. It seems plausible that higher concentrations of dSi should give rise to greater fractionation within the frustule, and vice versa. A recent study[43] suggested that dSi starvation can result in an increase in silicon content within the cell. This starvation response could potentially impact the isotopic composition of the resulting silica, by accentuating the kinetic fractionation effect. It would thus be of interest to examine the effect of dSi starvation on diatom isotopic fractionation, but to our knowledge such experiments have not yet been conducted.

In summary, our study confirms that Si isotopic fractionation in chemical experiments resembles that found in diatom silica from laboratory cultures and in the field. We also show that Si isotopic fractionation in the presence and absence of the R5 peptide is virtually indistinguishable. Our data confirm instead that the initial dSi concentration plays a major role in fractionation, with higher concentrations associated with increased $\Delta^{30}Si_{p\text{-}s}$. The initial stage of precipitation drives Si isotopic fractionation, and in our model system this initial fractionation is gradually attenuated by chemical equilibrium processes. This

leads to the proposition that the Si isotope fractionation factor in diatoms is not likely to be constant but instead is linked to a number of factors including external nutrients and internal cellular processes controlling dSi concentration within the cell. If the major control on internal dSi concentration is driven by the external environment, it is possible that diatom Si isotope archives used in palaeoenvironmental reconstructions could reveal more than just the biological consumption of dSi in surface oceans. They might also be useful means of understanding changes in diatom ecology due to environmental changes.

Methods

Experimental design

The media solution ND96 used during the experiment is composed of 47.8 $g.L^{-1}$ NaCl, 1.48 $g.L^{-1}$ KCl, 6.02 $g.L^{-1}$ MgCl2 and 5.95 $g.L^{-1}$ HEPES. The solution was adjusted with HCl or NaOH to obtain a final pH of 7.4. Sodium silicate solution (10% $Na_{2x}O$, 26.5% $Si0_2$) was added with different dilution factors to the ND96 buffer to cover a reasonable range of DSi concentrations to mimic the intra-cellular pools within diatoms[5,43]. The resulting concentrations being 743mM, 371mM, 148mM, 74.3mM, 37.1mM, 18.6mM, 7.4mM, 3.7mM. For all experiments and dilution factors, instantaneous precipitation was observed. For the biomimetic experiment, R5 was added to each sample at 0.01g/ml (5mM) before the addition of sodium silicate to ensure that the peptide is active[16]. The supernatant was sampled and separated from the precipitate at different times to evaluate the precipitation rates, solution/solid exchanges and the effect of the R5 peptide on the precipitation reactions and Si isotopic fractionation. The total volume for the abiotic and biomimetic was reduced to 1ml due to the mass of R5 peptide available. The volume limitation of the abiotic and biomimetic experiments other elemental analysis were not possible due to insufficient volume of solution. Table 2 summarises the details of the four different experimental set-ups.

Experiment	[dSi] (mM)	Total volume (ml)	Interval	Total time
8 Days	743, 371, 148, 74.3, 37.1, 18.6, 7.4, 3.7	10	/	8 days
1h	148, 74.3, 37.1, 18.6, 7.4, 3.7	10	/	1h
Abiotic	148, 74.3, 37.1, 18.6	1	1h, 1, 2, 4, 5, 6, 10 days	10 days
Biomimetic (R5)	148, 74.3, 37.1, 18.6	1	1h, 1, 2, 4, 5, 6, 10 days	10 days

Table 2. Experimental design

Si concentration and isotopes analysis

dSi analyses of the supernatant were carried out after each time step. Centrifugation (3000g for 5min) was carried before subsampling (at the surface of the supernatant) for dSi analysis to ensure no contamination from precipitate residue. dSi concentrations were measured using the silicomolybdate method[44], using a Agilent Cary 60 UV-Vis spectrophotomer for 8 days, 1h and using a nanodrop ND 1000 for the abiotic experiment, all at the wavelength of 410 nm. For the biomimetic (R5) experiment the dSi data have been extrapolated from the Multi Collector Induced Coupled Plasma Mass-Spectrometer (MC-ICP-MS) because R5 reacted with the colorimetric molybdate reagent. At the end of all experiment (total time), the supernatants and precipitates were separated by centrifugation. Precipitates were dissolved in 0.4N NaOH (Ananlar) at 100°C for 3 days and acidified with 6N HCl (in-house Teflon-distilled).

All samples were purified by cation exchange chromatography using Bio-Rad AG 50W X12, 200–400 mesh in H^+ form resin. δ^{30}Si analyses were carried out on the MC-ICP-MS (Finnigan Neptune s/n 1002, Bristol Isotopic Group). Measurement were operated on medium resolution and analysis were made on the low-mass side of the Si peaks where the polyatomic interferences (e.g. $^{14}N^{12}O$) were resolved from Si isotopes peaks. All sample analyses were at least duplicated and followed typical standard-sample bracketing and Mg doping methods[45]. The $\delta^{30}Si_{dSi}$ results are reported relative to the standard NBS28 (Equation 2). The measurement of the external standards LMG-08, with a mean value of -3.47 ± 0.17 ‰ (2 s.d., n = 37) and Diatomite, with a mean value of 1.24 ± 0.19 ‰ (2 s.d., n = 67) are in agreement with reference values[46,47]. For all samples and standards, the three isotopes (^{28}Si, ^{29}Si, ^{30}Si) were measured and results show good agreement with the mass-dependent fraction between δ^{29}Si and δ^{30}Si with $\delta^{29}Si = 0.511\ \delta^{30}Si$ (± 0.01).

$$\delta^{x}\mathrm{Si}(‰) = \left(\frac{\left(\frac{^{x}\mathrm{Si}}{^{28}\mathrm{Si}}\right)_{sample}}{\left(\frac{^{x}\mathrm{Si}}{^{28}\mathrm{Si}}\right)_{NBS28}} - 1 \right) \tag{2}$$

with x corresponding to ^{29}Si or ^{30}Si and NBS28 being the international Si standard Quartz NBS28 (RM8546).

Data availability

All data are presented in the supplementary information document.

References

1. Armbrust, E. V. The life of diatoms in the world's oceans. *Nature* **459**, 185–192, DOI: 10.1038/nature08057 (2009).
2. Sarmiento, J. L. & Orr, J. C. Three-dimensional simulations of the impact of Southern Ocean nutrient depletion on atmospheric CO2 and ocean chemistry. *Limnol. Oceanogr.* **36**, 1928–1950, DOI: 10.4319/lo.1991.36.8.1928 (1991).
3. Tréguer, P. & De La Rocha, C. L. The World Ocean Silica Cycle. *Annu. Rev. Mar. Sci.* **5**, 477–501 (2013).
4. Isson, T. T. *et al.* Evolution of the Global Carbon Cycle and Climate Regulation on Earth. *Glob. Biogeochem. Cycles* **34**, 1–28, DOI: 10.1029/2018GB006061 (2020).
5. Martin-Jézéquel, V., Hildebrand, M. & Brzezinski, M. A. Silicon metabolism in diatoms: Implications for growth. *J. Phycol.* **36**, 821–840, DOI: 10.1046/j.1529-8817.2000.00019.x (2000).
6. Thamatrakoln, K. & Hildebrand, M. Silicon uptake in diatoms revisited: a model for saturable and nonsaturable uptake kinetics and the role of silicon transporters. *Plant physiology* **146**, 1397–407, DOI: 10.1104/pp.107.107094 (2008).
7. Vrieling, E. G., Gieskes, W. W. & Beelen, T. P. M. Silicon deposition in diatoms: Control by the pH inside the silicon deposition vesicle. *J. Phycol.* **35**, 548–559, DOI: 10.1046/j.1529-8817.1999.3530548.x (1999).
8. Hildebrand, M. Diatoms, biomineralization processes, and genomics. *Chem. Rev.* **108**, 4855–4874, DOI: 10.1021/cr078253z (2008).
9. Heintze, C. *et al.* An intimate view into the silica deposition vesicles of diatoms. *BMC Mater.* **2**, 1–15, DOI: 10.1186/s42833-020-00017-8 (2020).
10. Kröger, N., Deutzmann, R., Bergsdorf, C. & Sumper, M. Species-specific polyamines from diatoms control silica morphology. *Proc. Natl. Acad. Sci. United States Am.* **97**, 14133–14138, DOI: 10.1073/pnas.260496497 (2000).
11. Wenzl, S., Hett, R., Richthammer, P. & Sumper, M. Silacidins: Highly acidic phosphopeptides from diatom shells assist in silica precipitation in vitro. *Angewandte Chemie - Int. Ed.* **47**, 1729–1732, DOI: 10.1002/anie.200704994 (2008).
12. Kröger, N., Deutzmann, R. & Sumper, M. Polycationic peptides from diatom biosilica that direct silica nanosphere formation. *Science* **286**, 1129–1132, DOI: 10.1126/science.286.5442.1129 (1999).
13. Kröger, N., Bergsdorf, C. & Sumper, M. Frustulin: domain conservation in a protein family associated with diatom cell walls. *Eur. J. Biochem.* **239**, 259–264 (1996).
14. Kröger, N., Lorenz, S., Brunner, E. & Sumper, M. Self-assembly of highly phosphorylated silaffins and their function in biosilica morphogenesis. *Science* **298**, 584–586, DOI: 10.1126/science.1076221 (2002).
15. Kröger, N., Deutzmann, R. & Sumper, M. Silica-precipitating peptides from diatoms: The chemical structure of silaffin-1A from Cylindrotheca fusiformis. *J. Biol. Chem.* **276**, 26066–26070, DOI: 10.1074/jbc.M102093200 (2001).
16. Senior, L. *et al.* Structure and function of the silicifying peptide R5. *J. Mater. Chem. B* **3**, 2607–2614, DOI: 10.1039/c4tb01679c (2015).
17. Knecht, M. R. & Wright, D. W. Functional analysis of the biomimetic silica precipitating activity of the R5 peptide from Cylindrotheca fusiformis. *Chem. Commun.* **3**, 3038–3039, DOI: 10.1039/b309074d (2003).
18. Marner, W. D., Shaikh, A. S., Muller, S. J. & Keasling, J. D. Morphology of artificial silica matrices formed via autosilification of a slilaffin/protein polymer chimera. *Biomacromolecules* **9**, 1–5, DOI: 10.1021/bm701131x (2008).
19. Lechner, C. C. & Becker, C. F. Modified silaffin R5 peptides enable encapsulation and release of cargo molecules from biomimetic silica particles. *Bioorganic Medicinal Chem.* **21**, 3533–3541, DOI: 10.1016/j.bmc.2013.04.006 (2013).
20. Lechner, C. C. & Becker, C. F. A sequence-function analysis of the silica precipitating silaffin R5 peptide. *J. Pept. Sci.* **20**, 152–158, DOI: 10.1002/psc.2577 (2014).
21. Buckle, E. L., Roehrich, A., Vandermoon, B. & Drobny, G. P. Comparative study of secondary structure and interactions of the R5 peptide in silicon oxide and titanium oxide coprecipitates using solid-state NMR spectroscopy. *Langmuir* **33**, 10517–10524, DOI: 10.1021/acs.langmuir.7b01048 (2017).
22. De La Rocha, C. L., Brzezinski, M. A. & DeNiro, M. J. Fractionation of silicon isotopes by marine diatoms during biogenic silica formation. *Geochimica et Cosmochimica Acta* **61**, 5051–5056, DOI: 10.1016/S0016-7037(97)00300-1 (1997).

23. Varela, D. E., Pride, C. J. & Brzezinski, M. A. Biological fractionation of silicon isotopes in Southern Ocean surface waters. *Glob. Biogeochem. Cycles* **18**, 1–8, DOI: 10.1029/2003GB002140 (2004).

24. Cardinal, D. *et al.* Relevance of silicon isotopes to Si-nutrient utilization and Si-source assessment in Antarctic waters. *Glob. Biogeochem. Cycles* **19**, 1–13, DOI: 10.1029/2004GB002364 (2005).

25. Grasse, P., Ehlert, C. & Frank, M. The influence of water mass mixing on the dissolved Si isotope composition in the Eastern Equatorial Pacific. *Earth Planet. Sci. Lett.* **380**, 60–71, DOI: 10.1016/j.epsl.2013.07.033 (2013).

26. Sutton, J. N. *et al.* A Review of the Stable Isotope Bio-geochemistry of the Global Silicon Cycle and Its Associated Trace Elements. *Front. Earth Sci.* **5**, 1–24, DOI: 10.3389/feart.2017.00112 (2018).

27. Gao, S., Wolf-Gladrow, D. A. & Völker, C. Simulating the modern δ30Si distribution in the oceans and in marine sediments. *Glob. Biogeochem. Cycles* **30**, 1–14, DOI: 10.1002/2015GB005189.Received (2016).

28. Panizzo, V. *et al.* Sea ice diatom contributions to Holocene nutrient utilization in East Antarctica. *Am. Geophys. Union* 1–15, DOI: 10.1002/2014PA002609.Received (2014).

29. Hendry, K. R. & Brzezinski, M. A. Using silicon isotopes to understand the role of the Southern Ocean in modern and ancient biogeochemistry and climate. *Quat. Sci. Rev.* **89**, 13–26, DOI: 10.1016/j.quascirev.2014.01.019 (2014).

30. Xiong, Z. *et al.* The silicon isotope composition of Ethmodiscus rex laminated diatom mats from the tropical West Pacific: Implications for silicate cycling during the Last Glacial Maximum. *Paleoceanography* **30**, 803–823, DOI: 10.1002/2015PA002793 (2015).

31. Dumont, M. *et al.* The nature of deep overturning and reconfigurations of the silicon cycle across the last deglaciation. *Nat. Commun.* **11**, 1–11, DOI: 10.1038/s41467-020-15101-6 (2020).

32. Hendry, K. R. *et al.* The biogeochemical impact of glacial meltwater from Southwest Greenland. *Prog. Oceanogr.* **176**, 102126, DOI: 10.1016/j.pocean.2019.102126 (2019).

33. Sutton, J. N., Varela, D. E., Brzezinski, M. A. & Beucher, C. P. Species-dependent silicon isotope fractionation by marine diatoms. *Geochimica et Cosmochimica Acta* **104**, 300–309, DOI: 10.1016/j.gca.2012.10.057 (2013).

34. Meyerink, S. W., Ellwood, M. J., Maher, W. A. & Strzepek, R. Iron availability influences silicon isotope fractionation in two Southern Ocean diatoms (Proboscia inermis and Eucampia antarctica) and a coastal diatom (Thalassiosira pseudonana). *Front. Mar. Sci.* **4**, 1–10, DOI: 10.3389/fmars.2017.00217 (2017).

35. Geilert, S., Vroon, P. Z., Roerdink, D. L., Van Cappellen, P. & van Bergen, M. J. Silicon isotope fractionation during abiotic silica precipitation at low temperatures : Inferences from flow-through experiments. *Geochimica et Cosmochimica Acta* **142**, 95–114, DOI: 10.1016/j.gca.2014.07.003 (2014).

36. Butler, I. B., Archer, C., Vance, D., Oldroyd, A. & Rickard, D. Fe isotope fractionation on FeS formation in ambient aqueous solution. *Earth Planet. Sci. Lett.* **236**, 430–442, DOI: 10.1016/j.epsl.2005.05.022 (2005).

37. Oelze, M., von Blanckenburg, F., Bouchez, J., Hoellen, D. & Dietzel, M. The effect of Al on Si isotope fractionation investigated by silica precipitation experiments. *Chem. Geol.* **397**, 94–105, DOI: 10.1016/j.chemgeo.2015.01.002 (2015).

38. Coradin, T., Eglin, D. & Livage, J. The silicomolybdic acid spectrophotometric method and its application to silicate / biopolymer interaction studies. *Spectroscopy* **18**, 567–576 (2004).

39. Stamm, F. M. *et al.* The experimental determination of equilibrium Si isotope fractionation factors among H4SiO4°, H3SiO4- and amorphous Silica (SiO2·0.32 H2O) at 25 and 75C using the three-isotope method. *Geochimica et Cosmochimica Acta* **255**, 49–68, DOI: 10.1016/j.gca.2019.03.035 (2019).

40. Pearce, C. R., Saldi, G. D., Schott, J. & Oelkers, E. H. Isotopic fractionation during congruent dissolution, precipitation and at equilibrium: Evidence from Mg isotopes. *Geochimica et Cosmochimica Acta* **92**, 170–183, DOI: 10.1016/j.gca.2012.05.045 (2012).

41. Cassarino, L., Hendry, K. R., Meredith, M. P., Venables, H. J. & De La Rocha, C. L. Silicon isotope and silicic acid uptake in surface waters of Marguerite Bay, West Antarctic Peninsula. *Deep. Res. Part II: Top. Stud. Oceanogr.* **139**, 143–150, DOI: 10.1016/j.dsr2.2016.11.002 (2017).

42. Meyerink, S. W. *et al.* Putting the silicon cycle in a bag: Field and mesocosm observations of silicon isotope fractionation in subtropical waters east of New Zealand. *Mar. Chem.* **213**, 1–12, DOI: 10.1016/j.marchem.2019.04.008 (2019).

43. Kumar, S., Rechav, K., Kaplan-Ashiri, I. & Gal, A. Imaging and quantifying homeostatic levels of intracellular silicon in diatoms. *Sci. Adv.* **6**, 1–8, DOI: 10.1126/sciadv.aaz7554 (2020).

44. Strickland, J. & Parsons, T. *A Practical Handbook of seawater analysis* (Fisheries Research Board of Canada, 1972), 2 edn. 1011.1669.

45. Cardinal, D., Alleman, L. Y., de Jong, J., Ziegler, K. & Andre, L. Isotopic composition of silicon measured by multicollector plasma source mass spectrometry in dry plasma mode. *J. Anal. At. Spectrom.* **18**, 213–218, DOI: 10.1039/b210109b (2003).

46. Reynolds, B. C. *et al.* An inter-laboratory comparison of Si isotope reference materials. *J. Anal. At. Spectrom.* **22**, 561–568, DOI: 10.1039/B616755A (2007).

47. Hendry, K. R. *et al.* Silicon isotopes in Antarctic sponges: an interlaboratory comparison. *Antarctic Sci.* **23**, 34–42 (2011).

Acknowledgements (not compulsory)

The authors would like to thank Sarah Ratcliffe for her help with initial experiment design and Christopher D. Coath for its support during mass spectrometry analysis. We acknowledge the funding from the Royal Society (Enhancement Award RG130386).

Author contributions statement

L.C., K.R.H. and P.C. conceived the experiments, L.C. conducted the experiments and analysed the results. All authors reviewed the manuscript.

Additional information

To include, in this order: **Accession codes** (where applicable); **Competing interests** (mandatory statement).

The corresponding author is responsible for submitting a competing interests statement on behalf of all authors of the paper. This statement must be included in the submitted article file.